TAUTZ, F. S., HEINE, V., DOVE, M. T. & CHEN, X. (1991). *Phys. Chem. Miner.* **18**, 326–336.
TRUEBLOOD, K. N. (1978). *Acta Cryst.* A**34**, 950–954.
URUSOV, V. S., DUBROVINSKII, L. S. & PILOYAN, G. O. (1986). *Dokl. Akad. Nauk. SSSR*, **288**, 126–129.
WILL, G., BELLOTTO, M., PARRISH, W. & HART, M. (1988). *J. Appl. Cryst.* **21**, 182–191.
WRIGHT, A. F. & LEHMANN, M. S. (1981). *J. Solid State Chem.* **36**, 371–380.
YOUNG, R. A. & POST, B. (1962). *Acta Cryst.* **15**, 337–346.

Acta Cryst. (1994). B**50**, 549–560

Inter-Relationship of Octahedral Geometry, Polyhedral Volume Ratio and Ferroelectric Properties in Rhombohedral Perovskites

BY NOEL W. THOMAS* AND ALI BEITOLLAHI

School of Materials, University of Leeds, Leeds LS2 9JT, England

(*Received* 24 *March* 1993; *accepted* 14 *March* 1994)

Abstract

A unifying, quantitative analytical framework has been developed for rhombohedral perovskite structures, ABO_3. Three principal parameters are defined: polyhedral volume ratio, V_A/V_B, mean octahedral tilt angle, $\langle\omega\rangle$, and octahedral distortion, Δs. The first two of these parameters are directly related through the equation $V_A/V_B = 6K\cos^2\langle\omega\rangle - 1$, with K practically invariant between all crystal structures. The four permutations of zero or non-zero $\langle\omega\rangle$ with zero or non-zero Δs are related to the four space groups in which rhombohedral perovskites crystallize, $R3m$, $R3c$, $R\bar{3}m$ and $R\bar{3}c$. The most general space group is $R3c$, which can accommodate non-zero values of both $\langle\omega\rangle$ and Δs. The structural driving force for non-zero Δs values (*i.e.* octahedral distortion) is examined by the bond-valence method, with the rationalization that octahedral distortions provide a mechanism for B-ion displacements which are parallel to one another and to the hexagonal z axis. Calculations of electrostatic energy further reveal the extra stabilization to be obtained by the adoption of electric dipole moments and parallel A- and B-ion displacements. It is these displacements which give rise to the ferroelectric properties of rhombohedral perovskites. The analysis is applied to the PZT system ($PbZrO_3$–$PbTiO_3$) and to the $PbZrO_3$–$BaZrO_3$ and $PbZrO_3$–$SrZrO_3$ systems. The influence of chemical composition on the relative stabilities of competing rhombohedral, orthorhombic and tetragonal phases is discussed, as is the physical basis of the morphotropic phase boundary in PZT. A method is also defined of predicting the temperatures at which the rhombohedral low-temperature phase in PZT transforms to the rhombohedral high-temperature phase, for a range of compositions.

* Author to whom correspondence should be addressed.

Introduction

The geometrical relationships governing the structures of rhombohedral perovskites, ABO_3, have been the focus of previous work (Michel, Moreau & James, 1971; Megaw & Darlington, 1975). The structural feature of most interest is the possible occurrence of BO_6 octahedral tilting, since this is thought to influence the ferroelectric, piezoelectric and electro-optic properties which can be shown by this class of materials. With the assumption of regular BO_6 octahedra, Michel *et al.* derived a relationship between hexagonal axial ratio c/a, octahedral tilt angle ω and rhombohedral cell angle α. A further relationship was derived, linking c/a with the positional parameter x of the anion $[x, 0, \frac{1}{4}]$ in position 18(*e*) ($R3c$, hexagonal). Megaw & Darlington subsequently proposed a more general parametrization, accommodating octahedral distortions and cation displacements explicitly. They considered the interrelationship between A-cation size, tilt angle, octahedron strain, and A- and B-cation displacements, and concluded that 'a single 'explanation' will not suffice for compounds so varied as the rhombohedral perovskites, in spite of their similar geometry.'

In this paper, however, it is shown that a single 'explanation' can indeed be given of the structures of rhombohedral perovskites. In particular, the ratio of the polyhedral volumes of the A- and B-cation polyhedra, V_A/V_B, can be correlated directly with octahedral tilt angle, ω. Whereas Megaw & Darlington failed to find a universal relationship between cation size† and tilt angle, such a relationship is derived in this work, where V_A/V_B is expressed as a function of ω. The effect of octahedral

† Megaw & Darlington (1975) used the parameter $(r_A + r_o)/l$ as a measure of 'ionic size', where r_A and r_o are the radii of A cations and oxygen anions, and l is the octahedron edge length.

©1994 International Union of Crystallography
Printed in Great Britain – all rights reserved

distortion on V_A/V_B is explicitly accommodated, and the link between octahedral distortion and B-ion displacement is elucidated by means of bond-valence analysis.

Method of calculation of ω, V_A and V_B

There are essentially two approaches towards calculating the octahedral tilt angle ω. The first of these would be to employ the known relationships linking ω with oxygen ion positional parameters (Megaw & Darlington, 1975). Alternatively, it is possible to construct three-dimensional computer-models of the structures, and to derive ω using methods of vector analysis. The latter approach was adopted here, since the associated molecular graphics techniques are helpful in visualizing structural features.

The occurrence of octahedral tilting in rhombohedral perovskites ABO_3 is shown in Fig. 1, for the case where all the triangular BO_6 octahedral faces are of equal edge-length. The influence of tilt angle on the geometry of A-ion coordination is emphasized in this figure. It is also possible for there to be two sets of triangular edge lengths, as shown in Fig. 2 for an arbitrary tilt angle, with an exaggerated inequality in triangular edge lengths. In general, the degree of irregularity in octahedral edge lengths is small, so it is appropriate to represent the two lengths as $s + \Delta s$ and $s - \Delta s$, with Δs the magnitude of the deviation of the edge lengths from a mean edge length, s.

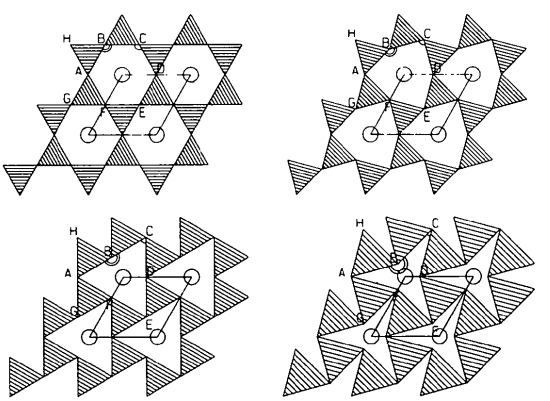

Fig. 1. Projections of the rhombohedral perovskite structure viewed along the z direction in hexagonal axes: (a) $\omega = 0°$; (b) $\omega = 15°$; (c) $\omega = 30°$; (d) $\omega = 45°$. The triangles represent co-planar faces of the BO_6 octahedra, which lie in the xy plane; A ions are represented as circles at the corners of the hexagonal unit cell, with the edge lengths of all triangles equal. In diagrams (b), (c) and (d), triangle AGF is rotated by $+\omega$ about its centre and triangle ABH by $-\omega$ with respect to the 0° orientations in diagram (a). Thus, angle BCD = 120° − 2ω and angle ABC = 120° + 2ω. The structure depicted in diagram (d) is not found in practice, since this is associated with concave A-ion coordination polyhedra (ABCDEF, in projection). Thus, there is an upper limit of $\omega = 30°$, as shown in diagram (c).

In Fig. 2 the larger octahedra are rotated clockwise and the smaller octahedra anticlockwise with respect to their untilted positions, but the inequality in edge lengths causes their respective angles of rotation to be unequal. If the angle of (clockwise) rotation of the larger octahedra is denoted by α and the angle of (anticlockwise) rotation of the smaller octahedra denoted by β, $\angle XYC = \alpha$ and $\angle YXC = \beta$. Since $XC = (s - \Delta s)/2$ and $YC = (s + \Delta s)/2$, it follows that

$$(s + \Delta s)\sin\alpha = (s - \Delta s)\sin\beta \quad (\alpha,\beta > 0). \qquad (1)$$

Note that when $\Delta s = 0$, β is equal to α, *i.e.* both sets of octahedra are rotated by equal angles, but in opposite senses. Although in general $\alpha \neq \beta$, the smallness of typical Δs values suggests that it is appropriate to define a mean tilt angle, $\langle\omega\rangle = (\alpha + \beta)/2$. $\langle\omega\rangle$ can be inferred directly from $\angle ABC$ and $\angle BCD$ in Fig. 2. It can be seen from simple geometry that $\angle ABC = 120° + (\alpha + \beta) = 120° + 2\langle\omega\rangle$ and that $\angle BCD = 120° - (\alpha + \beta) = 120° - 2\langle\omega\rangle$. Straightforward vector analysis enables these angles to be evaluated computationally (Thomas, 1992).

Values of V_A and V_B were calculated with a computer algorithm, as described previously (Thomas, 1991*a*). For the purposes of the present analysis, the coordination number of the A-ion is taken to be 12 in all structures. This is the natural choice in systems of low tilt angle, where a coordination cuboctahedron is formed, but not so obvious in systems with higher tilt. In Fig. 1(*a*), a cuboctahedron may be formed by taking co-planar vectices A, B, C, D, E and F and imagining two further triangles, one above the plane and one below (Thomas, 1991*b*). As the tilt angle is increased (ω is equal to 15° in Fig. 1*b* and 30° in Fig. 1*c*), vertices B, D and F coordinate the A-ion more closely than vertices A, C and E. Thus, the inplane coordination number falls from 6 to 3, with a corresponding reduction in three-dimensional coordination number from 12 to 9. For the purposes

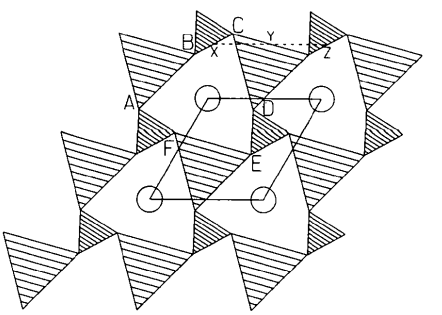

Fig. 2. Sketch of the structure for an arbitrary tilt angle, with BO_6 octahedra of unequal edge lengths. The straight line XYZ (of length equal to the lattice constant a) links mid-points of the sides of three triangles, with the angles within the triangle XYC defining tilt angles α and β.

of calculating V_A, however, it is appropiate to regard the coordination number as fixed at 12. This decision has been made for two reasons. First, a direct comparison between V_A/V_B ratios is to be made, and any dependence of V_A on coordination number would invalidate this. Secondly, a unique feature of perovskites is that the *B*-ion octahedra and *A*-ion cuboctahedra pack in such a way as to fill space. This permits a direct and useful relationship between coordination polyhedral volumes and unit-cell volumes (Thomas, 1989), which would no longer hold if an *A*-ion coordination number of less than 12 were adopted. In effect, void space would be introduced into the structures, an unnecessary complication.

Theoretical variation of V_A/V_B with ω

If Fig. 2 is considered, it is seen that the length of line XZ is equal to the unit-cell constant, a. Since $XZ = 2(XY)$, it follows that

$$(s + \Delta s)\cos\alpha + (s - \Delta s)\cos\beta = a. \quad (2)$$

As simplification of this equation is not straightforward, the development is best continued by considering the case when $\alpha = \beta(= \langle\omega\rangle)$. This condition is met whenever $\alpha = \beta = 0$ (therefore, $\langle\omega\rangle = 0$) or whenever the octahedral edge lengths are equal [$\Delta s = 0$, from (1)]. In such an instance, (2) reduces to $2s\cos\langle\omega\rangle = a$. This result can be generalized to layers with $\langle\omega\rangle > 0$ and $\Delta s \neq 0$ by the introduction of a factor K, such that

$$a = 2Ks\cos\langle\omega\rangle. \quad (3)$$

Thus, K is equal to unity for structures with $\Delta s = 0$ or $\langle\omega\rangle = 0$, and equal to $a/2s\cos\langle\omega\rangle$ in general.

The volume of an octahedron with trigonal symmetry can be expressed in terms of the edge lengths of the two equilateral triangular faces perpendicular to the triad axis, and the separation of these (Thomas, 1991*b*)

$$V_{oct} = (3^{1/2}d)/12(A + B)^2, \quad (4)$$

where A and B are the edge lengths of the two triangular faces and d is the separation of the two parallel faces, assumed to be equal to $c/6$, where c is the hexagonal cell constant. This step is a recognition that, in the vast majority of structures, the number of formula units in the unit cell, Z, = 6. Although the *R*3*m* structures have Z equal to 3, a straightforward doubling of length of the z axis is all that is required for Z to equal 6. It is also adequate to assume that the successive layers of oxygen ions perpendicular to the z axis are equally spaced. This is generally the case, apart from small deviations in a few structures. In structures with unequal edge-lengths, it is observed that $A = s - \Delta s$ and $B = s + \Delta s$, since the two faces perpendicular to the z axis consist of one larger and one smaller face. Thus, the octahedral volume of the B cations, V_B, = $3^{1/2}cs^2/18$. Given that the volume of the unit cell is equal to $3^{1/2}a^2c/2$, Z = 6, and the A and B polyhedra fill space, it follows that

$$V_A = (3^{1/2}a^2c)/6.2 - (3^{1/2}cs^2)/18. \quad (5)$$

On substituting for s in terms of a and ω from (3), and simplifying the algebra, the following relationship is obtained

$$V_A/V_B = 6K^2\cos^2\langle\omega\rangle - 1. \quad (6)$$

This relationship links the polyhedral volume ratio V_A/V_B directly with the tilt angle ω. The exact value of K is given by (3), with K either exactly or approximately equal to 1.

Examination of experimentally determined structures

Table 1 gives the calculated values of V_A, V_B, V_A/V_B and $\langle\omega\rangle$ for 29 rhombohedral structures retrieved from the Inorganic Crystal Structure Database (ICSD). Other columns contain the temperatures of the samples at which the diffraction data were collected, rhombohedral lattice strain, $90 - \alpha$, s, Δs, unit-cell constant a, and the value of K, as calculated from (3).

The relationship between $\langle\omega\rangle$ and V_A/V_B

The validity of the relationship between $\langle\omega\rangle$ and V_A/V_B proposed in (6) may be investigated by plotting the experimental V_A/V_B ratios against $\langle\omega\rangle$ for all the structures in Table 1 (Fig. 3). The curve which is fitted corresponds to the function $6\cos^2\langle\omega\rangle - 1$, *i.e.* (6), with $K = 1$. Since K is so close to 1 in all structures (see Table 1), it is not surprising that this curve is an excellent fit.

Owing to small deviations from idealized equispacing of oxygen layers in some structures, some of

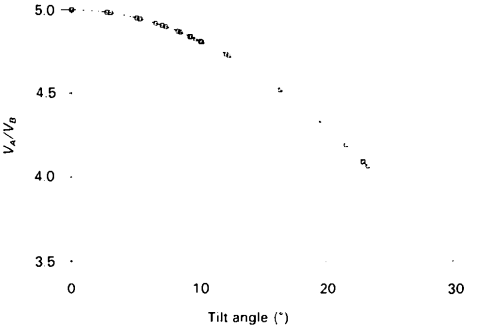

Fig. 3. Plot of V_A/V_B *versus* tilt angle, ω. The theoretical variation [(6), with $K = 1$] is represented by the continuous line, with experimental points (see Table 1) represented as small squares.

Table 1. *Experimental crystallographic data for rhombohedral perovskites, with calculated values of* $\langle\omega\rangle$, V_A, V_B, V_A/V_B, s, Δs *and* K

Composition	ICSD No.	Temperature (K)	SG	$90-\alpha$ (°)	$\langle\omega\rangle$ (°)	V_A (Å^3)	V_B (Å^3)	V_A/V_B	s	Δs	a	K	References
PZT (0.9)*	1263	293	161	0.279	5.419	59.036	11.935	4.947	2.9336	0.10089	5.841	1.00001	(1)
PZT (0.9)	1264	333	161	0.282	6.634	59.048	12.001	4.920	2.9412	0.07980	5.843	1.00000	(1)
PZT (0.9)	1265	373	160	0.265	0.000	59.333	11.867	5.000	2.9240	0.07339	5.848	1.00000	(1)
PZT (0.9)	1266	423	160	0.240	0.000	59.386	11.877	5.000	2.9255	0.03832	5.851	1.00000	(1)
PZT (0.9)	1267	473	160	0.194	0.000	59.406	11.881	5.000	2.9270	0.03132	5.854	1.00000	(1)
PZT (0.9)	1268	508	160	0.135	0.000	59.376	11.875	5.000	2.9280	0.02430	5.856	1.00000	(1)
$LaCuO_3$	3736	1173	167	−0.733	7.109	47.958	9.771	4.908	2.7718	0.0	5.501	1.00000	(2)
$KNbO_3$	3839	230	160	0.183	0.000	53.975	10.795	5.000	2.8352	0.01815	5.670	1.00000	(3)
$LiTaO_3$	3843	297	161	3.450	22.876	42.476	10.374	4.095	2.7968	0.07314	5.154	1.00006	(4)
$NdAlO_3$	4596	293	167	−0.353	10.134	43.721	9.082	4.814	2.7032	0.0	5.322	1.00000	(5)
$BiFeO_3$	5525	293	161	0.499	12.326	51.587	10.913	4.727	2.8598	0.09827	5.588	1.00009	(6)
$HgTiO_3$	7416	298	161	1.242	16.407	46.506	10.286	4.521	2.8032	0.0	5.378	1.00000	(7)
PZT (0.58)	10309	293	160	0.350	0.000	56.179	11.236	5.000	2.8691	0.33282	5.738	1.00000	(8)
$NaNbO_3$	13245	123	161	0.780	12.140	49.284	10.407	4.735	2.8075	0.10734	5.490	1.00009	(9)
$LiUO_3$	13598	293	161	4.940	22.910	51.032	12.475	4.091	2.9383	0.0	5.413	1.00000	(10)
$LiReO_3$	17290	293	161	2.811	21.554	40.499	9.661	4.192	2.7372	0.08525	5.092	1.00007	(11)
$LiNbO_3$	17292	293	161	3.728	23.262	42.560	10.469	4.065	2.8016	0.07237	5.148	1.00006	(11)
$NdAlO_3$	17685	293	167	−0.347	9.383	43.719	9.032	4.841	2.6961	0.0	5.320	1.00000	(12)
$PrAlO_3$	17790	293	166	−0.285	0.000	44.366	8.873	5.000	2.6667	0.0	5.333	1.00000	(13)
PZT (0.9)	20625	293	161	0.289	2.772	59.131	11.859	4.986	2.9239	0.12982	5.841	1.00000	(14)
PZT (0.75)	28925	83	161	0.348	5.156	57.580	11.628	4.952	2.9061	0.12107	5.789	1.00001	(15)
PZT (0.75)	28926	293	161	0.296	3.078	57.779	11.596	4.983	2.9022	0.11286	5.796	1.00000	(15)
PZT (0.75)	28927	378	160	0.270	0.000	57.854	11.571	5.000	2.8994	0.12178	5.799	1.00000	(15)
$LaCoO_3$	25290	4	167	−0.849	10.240	45.616	9.483	4.810	2.7545	0.0	5.422	1.00000	(16)
$LaCoO_3$	25291	71	167	−0.829	10.173	45.776	9.511	4.813	2.7568	0.0	5.427	1.00000	(16)
$LaCoO_3$	25292	293	167	−0.686	9.769	46.377	9.607	4.827	2.7614	0.0	5.443	1.00000	(16)
$LaCoO_3$	25293	668	167	−0.516	9.315	47.709	9.852	4.843	2.7784	0.0	5.485	1.00000	(16)
$LaCoO_3$	25295	1143	167	−0.308	8.501	49.194	10.104	4.869	2.7947	0.0	5.530	1.00000	(16)
$LaCoO_3$	25296	1248	167	−0.256	8.346	49.538	10.165	4.874	2.7992	0.0	5.540	1.00000	(16)

* PZT (x) has the composition $Pb(Zr_xTi_{1-x})O_3$.

References (in CODEN form): (1) ACBCA 34 1060 1978; (2) MRBUA 7 913 1972; (3) JPSOA 6 2559 1973; (4) JPCSA 28 1685 1967; (5) JSSCB 4 11 1972; (6) JPCSA 32 1315 1971; (7) JSSCB 6 509 1973; (8) SSCOA 7 865 1969; (9) ACBCA 29 2171 1973; (10) ZAACA 338 9 1965; (11) JSSCB 42 251 1982; (12) ACSCE 39 673 1983; (13) ACCRA 9 1019 1956; (14) JUPSA 52 913 1983; (15) FEROA 82 79 1988; (16) JSSCB 61 301 1986.

the calculated V_A and V_B values in the table are averages. This is not of any significance, however, since deviations from the average are so small, typically 0.001 Å^3 in V_B values and 0.01 Å^3 in V_A values. From (6), the range of allowed tilt angles between 0 and 30° implies that the range of allowed V_A/V_B ratios corresponds to $3.5 \leq V_A/V_B \leq 5$. Note that the maximum experimentally observed value of $\langle\omega\rangle$ is found in $LiNbO_3$, with $\langle\omega\rangle = 23.262°$; the corresponding V_A/V_B ratio is 4.065.

Space group

As discussed previously (Megaw & Darlington, 1975), the predominant space groups in rhombohedral perovskites are 160, 161 and 167 ($R3m$, $R3c$ and $R\bar{3}c$, respectively), with $PrAlO_3$ crystallizing in space group 166 ($R\bar{3}m$). The particular space group adopted reflects the geometrical relationship between the oxygens ions in successive layers. In space group 160, successive AO_3 layers are generated merely from the translations associated with hexagonal axes, $[\frac{1}{3},\frac{2}{3},\frac{2}{3}]$ and $[\frac{2}{3},\frac{1}{3},\frac{1}{3}]$, giving three AO_3 layers per unit cell. In the other three space groups, the (x,y) coordinates in adjacent AO_3 layers are related by a rotation, reflection or inversion operation. In $R3c$ (161), this operation corresponds to reflections in the (110) plane, in $R\bar{3}m$ (166) an inversion, and in $R\bar{3}c$ (167) a 180° rotation about the z axis. The incorporation of this operation in addition to the hexagonal translations necessarily increases the number of layers in the unit cell to six.

Fig. 4 demonstrates the four possible geometrical relationships between adjacent AO_3 layers. For illustrative purposes, the AO_3 layers are made up of two differently sized O_3 triangular faces, with one side two thirds the length of the other. A mean tilt angle of 19° has also been chosen. In Fig. 4(*a*), a simple hexagonal translation relates the two layers, as in space group 160 ($R3m$). It is seen that the larger triangular faces always lie above the smaller faces, so that all the octahedra are geometrically equivalent. However, the non-zero tilt angle gives rise to distorted octahedra, which would be structurally unfavourable. It is concluded, therefore, that space group 160 is appropriate for structures with $\Delta s \neq 0$, provided that the tilt angle is zero. This conclusion is borne out by all the structures in Table 1 with the $R3m$ space group, where $\langle\omega\rangle = 0$ and $\Delta s \neq 0$.

In Fig. 4(*b*), the adjacent layers are related by a (110) reflection plus translation, as in space group 161. As in Fig. 4(*a*), the BO_6 octahedra are formed by one smaller and one larger O_3 triangle ($\Delta s \neq 0$). In this case, the angular dispositions of the oxygen octahedral vertices are more regular, in spite of the tilting. It is concluded, therefore, that space group

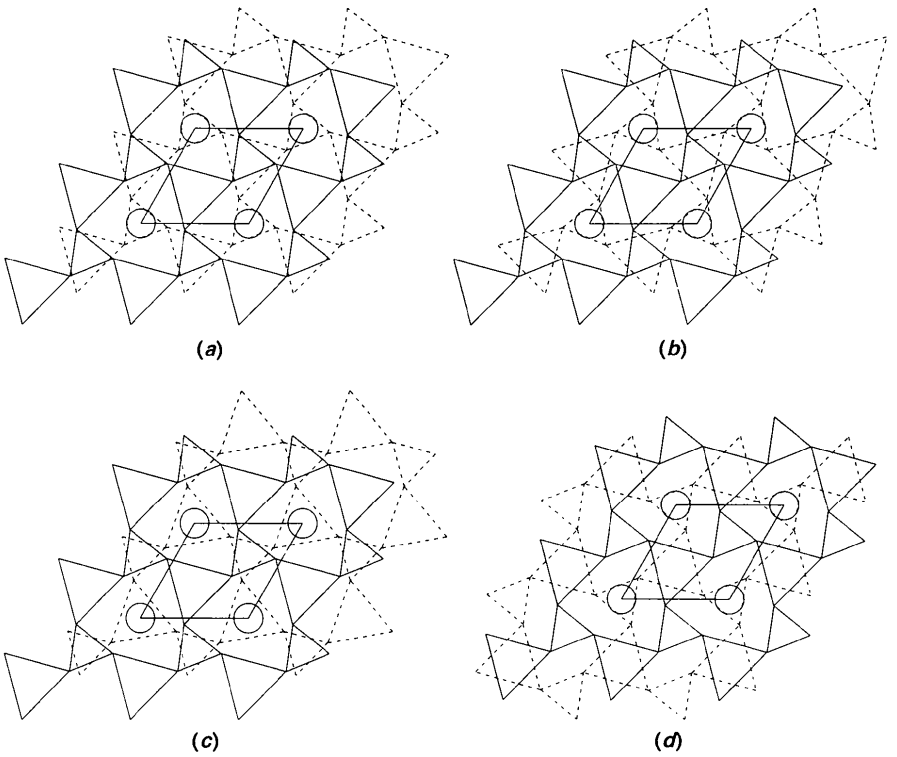

Fig. 4. The relative disposition of two adjacent AO_3 layers with $\Delta s \neq 0$ and $\langle\omega\rangle \neq 0$, represented as O_3 triangular faces of the BO_6 octahedra. The lower layer (full lines) and the upper layer (dashed lines) can be related by four different symmetries: (*a*) hexagonal translation (as in SG 160); (*b*) (110)-reflection + translation (as in SG 161); (*c*) inversion + translation (as in SG 166); (*d*) 180° rotation about the z axis + translation (as in SG 167).

Table 2. *Summary of values of* $\langle\omega\rangle$ *and* Δs *in space groups R3m, R3c, R$\bar{3}$m and R$\bar{3}$c*

Space group	Number	Allowed values of $\langle\omega\rangle$ and Δs	
R3m	160	$\langle\omega\rangle = 0$	$\Delta s \neq 0$
R3c	161	$\langle\omega\rangle \neq 0$	$\Delta s \neq 0$
R$\bar{3}$m	166	$\langle\omega\rangle = 0$	$\Delta s = 0$
R$\bar{3}$c	167	$\langle\omega\rangle \neq 0$	$\Delta s = 0$

161 (*R3c*) is appropriate for structures with a non-zero tilt angle and unequal octahedral edge lengths, *i.e.* when both $\langle\omega\rangle$ and Δs are non-zero.

In Fig. 4(*c*), the two AO_3 layers are related by inversion and translation, as in space group 166 (*R$\bar{3}$m*). Not only are the octahedral vertices at irregular angles as a result of the tilting, but smaller faces lie above smaller faces and larger above larger. Thus, if Δs were non-zero, the volumes of the two types of octahedron would differ. Since both of these are unfavourable structural features, it is argued that space group 166 is associated only with structures with a zero tilt angle and zero Δs. This is borne out by the $PrAlO_3$ structure in Table 1.

In Fig. 4(*d*), successive AO_3 layers are related by a rotation followed by a translation, as in space group 167 (*R$\bar{3}$c*). The formation of octahedra from (large + large) and (small + small) faces dictates that $\Delta s = 0$, but $\langle\omega\rangle$ can be non-zero, as the angular geometry of these octahedra is regular.

The above conclusions are summarized in Table 2. The significance of non-zero values of Δs for the occurrence of *B*-ion displacements is brought out in the following section.

Cation displacements and octahedral distortions

A further feature of these structures concerns the displacements of the *A* and *B* cations relative to the centres of coordinates of the coordination polyhedra. These are crucial to the occurrence of ferroelectricity (and related phenomena) in rhombohedral perovskites.

The magnitudes of the cation displacements are quoted in Table 3, in the columns headed Δz_A and Δz_B. All non-zero displacements are parallel to the threefold axis (the *z* axis), with *A*- and *B*-ion displacements parallel to each other. In order to monitor the short-range forces governing cationic displacements, use is made of the bond-valence method, with the results also quoted in Table 3. The bond-valence parameters employed correspond to the (R_o,N) formalism, *i.e.* bond strength $s = (R/R_o)^{-N}$, wherever the appropriate parameters are available (Brown, 1981). In other cases, (r_o,B) parameters have been used in connection with the relationship $s = \exp[(r_o - r)/B]$, with values of r_o and *B* taken from Brown & Altermatt (1985). The (R_o,N) parameters were found, in general, to give more realistic valences for the structures in Table 3, particularly with respect to the *A* ions.

The columns headed v_A and $v_{A,\mathrm{cen}}$ in Table 3 contain valences calculated by the bond-valence method for the *A* ions at their experimentally determined positions and at the centres of coordinates of their 12-fold coordination polyhedra. Thus, in all cases where $\Delta z_A = 0$, $v_A = v_{A,\mathrm{cen}}$. A consideration of $v_{A,\mathrm{cen}}$ values reveals that a valence deficiency for the cation at the centre of its coordination polyhedron (*i.e.* $v_{A,\mathrm{cen}} < v_{\mathrm{ideal}}$) gives rise to a displacement of that cation (*i.e.* $\Delta z_A \neq 0$). For example in $BiFeO_3$, $v_{a,\mathrm{cen}} = 2.5171$, corresponding to a valence deficiency of 0.4829 against the idealized bismuth valency of 3. Following a displacement of $\Delta z_A = 0.6337$ Å, this deficiency is reduced to 0.0516 ($v_A = 2.9484$). Conversely, a valence excess of an *A* cation at the centre of its coordination polyhedron ($v_{A,\mathrm{cen}} > v_{\mathrm{ideal}}$) is generally associated with no off-centre displacement, *i.e.* $\Delta z_A = 0$. This is found in $HgTiO_3$, $NdAlO_3$ and $PrAlO_3$. Exceptions to these generalizations are found in $KNbO_3$, where the available bond-valence parameters give rise to valences which are too high, and in the structures of $LiUO_3$ and $LiNbO_3$, where the large values of Δz_A entail significant changes in coordination as the lithium cation is displaced from the centre of its 12-fold coordination polyhedron.

The *B*-ion valences for PZT compositions are contained in six columns, rather that two, reflecting the statistical occupation of *B* sites by both zirconium and titanium ions. Thus, the columns headed $v_{B,1}$ and $v_{B,2}$ list zirconium and titanium valences, respectively, with the $\langle v_B\rangle$ column containing an averaged valence of $x.v_{B,1} + (1 - x).v_{B,2}$ for the composition $Pb(Zr_xTi_{1-x})O_3$. The three right-hand columns with a 'cen' subscript list calculated valences for the *B* ions when situated at the centres of coordinates of their octahedral coordination polyhedra.

Three basic patterns are observed: structures for which (i) $v_{B,\mathrm{cen}} < v_B$, (ii) $v_{B,\mathrm{cen}} = v_B$ and (iii) $v_{B,\mathrm{cen}} > v_B$. Structures in the first category are $KNbO_3$, $NaNbO_3$, $LiNbO_3$ and PZT (0.9; ICSD No. 20625). Of these four, $KNbO_3$, $NaNbO_3$ and PZT (ICSD No. 20625) have anomously high valences in one site, the *A* site in $KNbO_3$ and the *B* site in $NaNbO_3$ and PZT. It is likely, therefore, that the K—O bond-valence parameters are inappropriate for $KNbO_3$. However, the high values of $\langle V_B\rangle$, 4.6993 for PZT (ICSD No. 20625) and 5.6348 for $NaNbO_3$, are suggestive of inaccurate crystal structures. This is particularly likely for the PZT structure, since a study of this composition at the same temperature by other workers (PZT, ICSD No. 1263) gives rise to an acceptable value for $\langle v_B\rangle$ of 3.9615. Since in the third structure of the first category, $LiNbO_3$, the magni-

Table 3. *Displacements of A and B ions, Δz_A and Δz_B, together with their calculated valences, both in experimentally determined positions and when located at the centres of their coordination polyhedra*

Composition	ICSD No.	Δz_A (Å)	Δz_B (Å)	v_A	$v_{A,cen}$	$v_{B,1}$	$v_{B,2}$	$\langle v_B \rangle$	$v_{B,1,cen}$	$v_{B,2,cen}$	$\langle v_{B,cen} \rangle$
PZT (0.9)	1263	0.4559	0.1648	1.9304	1.7030	4.0816	2.8802	3.9615	4.1592	2.9276	4.0360
PZT (0.9)	1264	0.4431	0.1619	1.9176	1.7198	4.0613	2.8667	3.9418	4.0974	2.8910	3.9768
PZT (0.9)	1265	0.3842	0.1375	1.8101	1.6540	4.1513	2.9231	4.0285	4.1868	2.9459	4.0627
PZT (0.9)	1266	0.3711	0.1116	1.7813	1.6511	4.1696	2.9341	4.0461	4.1630	2.9326	4.0400
PZT (0.9)	1267	0.2642	0.1042	1.7154	1.6501	4.1699	2.9344	4.0464	4.1583	2.9299	4.0355
PZT (0.9)	1268	0.2106	0.0307	1.6927	1.6516	4.1560	2.9288	4.0333	4.1609	2.9316	4.0380
$LaCuO_3$	3736	0.0000	0.0000	2.8006	2.8006						
$KNbO_3$	3839	0.1268	0.2175	1.6347	1.6021			4.8601			4.6366
$LiTaO_3$	3843	0.6014	0.2017	0.9811*	0.9975*			4.9659			4.9726
$NdAlO_3$	4596	0.0000	0.0000	3.2946	3.2946			3.0959*			3.0959*
$BiFeO_3$	5525	0.6337	0.2344	2.9484	2.5171			2.9564			2.9845
$HgTiO_3$	7416	0.0000	0.0000	2.1991	2.1991			3.7590			3.7590
PZT (0.58)	10309	0.2317	0.1324	1.9840	1.8326	4.6283	3.2052	4.0306	5.1911	3.5116	4.4857
$NaNbO_3$	13245	0.3476	0.2721	1.1191*	1.0859*			5.6348			4.9703
$LiUO_3$	13598	1.0512	0.0000	0.7075*	0.7322*			5.8639*			5.8639*
$LiReO_3$	17290	0.3619	0.0000	1.0094*	1.0030*						
$LiNbO_3$	17292	0.6945	0.2787	0.9976*	1.0231*			4.9751			4.8970
$NdAlO_3$	17685	0.0000	0.0000	3.2468	3.2468			3.1255*			3.1255*
$PrAlO_3$	17790	0.0000	0.0000	3.0077	3.0077			3.2227*			3.2227*
PZT (0.9)	20625	0.4936	0.2181	1.7999	1.6734	4.8547	3.3010	4.6993	4.2401	2.9748	4.1136
PZT (0.75)	28925	0.4879	0.1717	2.0709	1.7797	4.2763	2.9995	3.9571	4.4023	3.0738	4.0702
PZT (0.75)	28926	0.4478	0.1431	1.9942	1.7478	4.3075	3.0198	3.9856	4.4184	3.0842	4.0849
PZT (0.75)	28927	0.4041	0.1073	1.9429	1.7328	4.3298	3.0348	4.0061	4.4464	3.1006	4.1100
$LaCoO_3$	25290	0.0004	0.0000	3.2856	3.2856						
$LaCoO_3$	25291	0.0000	0.0000	3.2568	3.2568						
$LaCoO_3$	25292	0.0000	0.0000	3.1443	3.1443						
$LaCoO_3$	25293	0.0013	0.0000	2.9351	2.9351						
$LaCoO_3$	25295	0.0013	0.0000	2.7108	2.7109						
$LaCoO_3$	25296	0.0004	0.0000	2.6642	2.6642						

* Valence sum calculated with (r_o,B) parameters (Brown & Altermatt, 1985).

tude of Δz_B, 0.2787 Å, is the largest of all the structures, the observation that $v_{B,cen}$ is less than v_B can be attributed solely to this large displacement.

It is concluded, therefore, that structures in the first category are an exception to a general rule for rhombohedral perovskites, which states that $v_{B,cen} \geq v_B$. The structural basis for this rule lies in the octahedral distortions ($\Delta s \neq 0$) to be found in all the structures for which $v_{B,cen} > v_B$. In a distorted octahedral environment of this kind, the B ion is displaced off-centre towards the larger octahedral face, of edge length $s + \Delta s$ and away from the smaller face, of length $s - \Delta s$. If at the centre of its coordinating octahedron, the cation would have a higher calculated valence, owing to shorter interaction lengths with the three oxygen ions in the smaller face. In moving off-centre, the interaction lengths with the oxygen ions in the smaller face are increased, whereas the interaction lengths with the three oxygen ions in the larger face, which are inherently longer, do not decrease sufficiently for v_B to increase relative to $v_{B,cen}$.

The widespread occurrence of this octahedral distortion in rhombohedral perovskites merits further consideration, since it has a direct influence on the occurrence of ferroelectricity in these compounds. As a consequence of the alternation between large and small octahedral faces within each AO_3 layer (Fig. 4) and the displacement of the AO_3 layers relative to one another, all of the larger faces, as drawn in Fig. 4(*b*), lie above the smaller faces. Recall that Fig. 4(*b*) relates to space group $R3c$, in which both octahedral tilting and octahedral distortions can be accommodated. It serves, therefore, as a generalized case. Since a larger face always lies above a small face in a structure with octahedral distortions, it follows that all the B ions are displaced from their octahedral centres in the same direction, towards the larger faces (*i.e.* perpendicular to, and out of the plane of the paper). Thus, this octahedral distortion acts as a mechanism whereby all the B-ion displacements are constrained to be parallel to one another. A unique direction for the polar axis is thereby created by this 'structural coupling' of B-ion displacements.

Coupling between A and B cationic displacements: calculation of electrostatic energies

A further issue worthy of consideration relates to the displacements of the A ions from the centres of their 12-fold coordination polyhedra. As discussed above, $v_{A,cen} < v_A$, and the off-centre displacement is connected with obtaining calculated A-ion valences closer to ideal values. However, the bond-valence analysis relates to nearest-neighbour cation–anion interactions only, and the A ions can achieve idealized valences by displacements which are either parallel or antiparallel to the B-ion displacements. A

question arises, therefore, as to why the *A*-ion displacements are parallel to the *B*-ion displacements in these structures, so that both *A* and *B* ions contribute to the spontaneous polarization of these crystals in the same sense.

To tackle this question, the electrostatic potential energy is now calculated in two representative rhombohedral perovskites, PZT (0.9; ICSD No. 1263) and $BiFeO_3$ (ICSD No. 5525). This energy is calculated by assigning point charges to ions, and evalulating the pairwise sum $S_1 = \sum_{j \neq k}(q_j q_k)/r_{jk}$, where j and k refer to different ions, and r_{jk} is their interaction length. Note that this sum does not represent the true potential energy of the crystal, since no account has been taken of the following two factors: (i) short-range electron-overlap repulsive forces and (ii) the departure of electronic charge distributions from spherical symmetry. Such departures will be due to partially covalent interactions and to the polarizability of valence orbitals. Whereas a partial accommodation of these factors could be effected by reducing the magnitudes of the point charges on anions and cations, there is no straightforward method of estimating the reductions required. The calculated electrostatic energies are thus to be interpreted only comparatively, as the sum S_1 is adequate to reveal differences in the electrostatic stabilization of a structure as a given feature, such as *A*-ion displacement, is varied.

Since electrostatic forces have a long range, the sum S_1 converges very slowly, and an appropriate convergence acceleration technique is used. The method employed here was advocated by Williams (1971), with the following parametrization

$$S_1 = \sum_{j \neq k} q_j q_k r_{jk}^{-1}\,\mathrm{EFRC}(a) + 1/(2\pi V)\sum_{h_\lambda \neq 0} |F(\mathbf{h}_\lambda)|^2 h_\lambda^{-2} \exp(-b^2) - K\sum_{\text{cell}} q_j^2. \quad (7)$$

In the first term, q_j and q_k are ionic charges, r_{jk} their separation; ERFC(a) is the complementary error function for the argument a, defined by

$$a^2 = \pi K^2 r_{jk}^2 . \quad (8)$$

K is a convergence constant, typically set to a value between 0.2 and 0.4. In this work, the energy sum is calculated with three values of K, 0.2, 0.3 and 0.4. In the second term, V is the unit-cell volume, $F(\mathbf{h}_\lambda)$ the structure factor at reciprocal lattice points $\mathbf{h}_\lambda$, which is defined by

$$F(\mathbf{h}) = \sum_{\text{cell}} q_j \exp(-2\pi \mathbf{h}.\mathbf{r}_j). \quad (9)$$

The parameter b is given by

$$b^2 = (\pi h_\lambda^2)/K^2. \quad (10)$$

Table 4. *Electrostatic energies calculated according to* (7), *for three different values of the convergence constant, K*

System	Calculated electrostatic energy (kJ mol^{-1})* $K = 0.2$	$K = 0.3$	$K = 0.4$
PZT (0.9; ICSD No. 1263)	−16640.443	−16640.437	−16640.437
$BiFeO_3$ (ICSD No. 5525)	−15890.434	−15890.431	−15890.432
$BiFeO_3$ (dipole moments zero)	−15654.888	−15654.879	−15654.879

* A relative permittivity, ε_r, equal to 1 has been assumed.

The parameters K and q_j, which appear in the third term, have already been defined.

The electrostatic energy has been calculated for three static systems, (i) the experimentally determined structure of PZT (0.9; ICSD No. 1263), (ii) the experimentally determined structure $BiFeO_3$ (ICSD No. 5525) and (iii) $BiFeO_3$ with Bi and Fe displacements along the former polar axis reduced to zero. Thus, the electrostatic energy in the absence of electric dipole moments is calculated. The results are quoted in Table 4 for three values of the convergence parameter K. The agreement between the values is indicative that the algorithm employed (Thomas, 1993) is functioning correctly. In calculating these energies according to (7), r_{jk} values up to a cutoff of 8 Å were taken for the first term, with reciprocal lattice vectors of magnitude up to 1 Å^{-1} taken in the second term. These cutoffs are more than adequate to ensure convergence of the summation. In quoting the calculated energies in kJ mol^{-1}, a relative permittivity of one has been adopted. Although this is an underestimate, leading to calculated energies which are too large, this is a systematic error, which will not invalidate the comparisons to be made.

By comparing values of electrostatic energy for the experimental structure of $BiFeO_3$ and the simulated structure with dipole moments of zero (Table 4), it is clear that the existence of the dipole moments provides an extra stabilization energy. A pointer to why *A* and *B* ionic displacements are parallel to one another is also given by calculations of electrostatic energy. The results are presented graphically in Fig. 5 for PZT (0.9; ICSD No. 1263) and $BiFeO_3$. The displacement on the abscissa refers to the distance of the *A* ion (Pb and Bi, respectively) from the plane of oxygen ions. Thus, a positive displacement signifies that the *A*- and *B*-ion displacements are parallel, whereas a negative displacement indicates antiparallel *A*- and *B*-ion displacements. It is clear from both graphs that electrostatic energy considerations favour parallel *A*- and *B*-ion displacements, as is found experimentally. Clearly greater electrostatic stabilization could be achieved by larger *A*-ion displacements than are observed experimentally, but these would be at the expense of increased short-range ionic repulsions, which are not calculated here.

An overall picture of the creation of polar structures in rhombohedral perovskites may thus be formulated. The distortion on the oxygen ions in the BO_6 octahedra provides a means whereby all the B ions are displaced parallel to the hexagonal z axis without unfavourable short-range ionic interactions (as monitored by the bond-valence method). Greater electrostatic stabilization is associated with the formation of electric dipoles, as is the adoption of parallel A- and B-ion displacements.

It is likely that the extra electrostatic stabilization to be gained by the existence of dipole moments ($\Delta z_B > 0$) is a driving force for the observed octahedral distortions. This is supported by a bond-valence calculation on the PZT system (0.58), where the octahedral distortion, Δs, is greatest. If this structure were to adopt regular octahedra ($\Delta s = 0$) of volume equal to that of the distorted octahedra (11.236 Å^3, see Table 1), the six Zr/Ti interaction lengths would be equal to 2.035 Å, with the corresponding weighted Zr/Ti bond-valence sum $\langle V_B \rangle = 4.0531$. Since this is virtually identical to the $\langle V_B \rangle$ value of the actual distorted octahedron, 4.0306, it is inferred that short-range interactions do not favour the distorted octahedron any more than the regular one. It is only the increased electrostatic stabilization which can provide a driving force for the octahedral distortion.

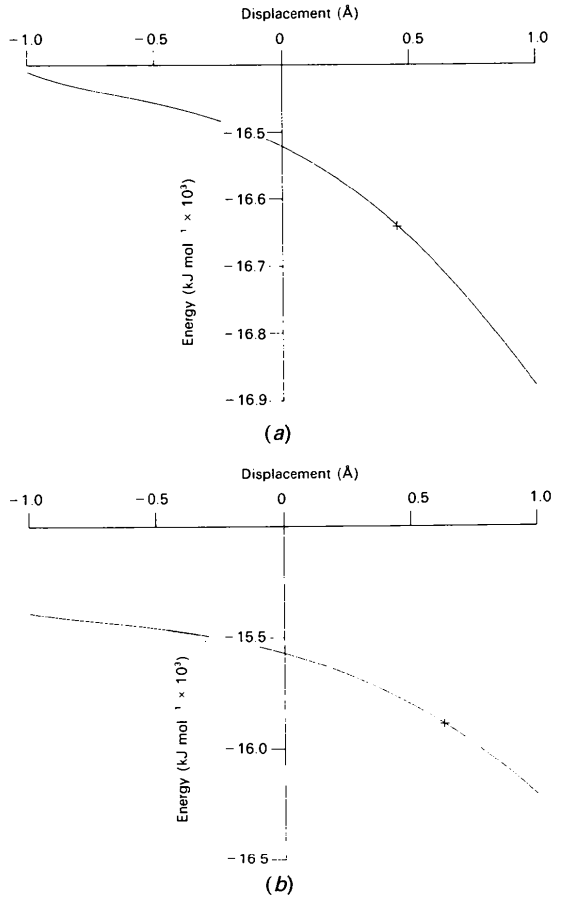

Fig. 5. Variation of electrostatic energy (7) *versus* displacement of A ions from the plane of oxygen ions for (*a*) PZT (0.9; ICSD No. 1263) and (*b*) $BiFeO_3$ (ICSD No. 5525). The energies of the experimental structures are denoted by crosses. A positive displacement signifies that A- and B-ion displacements are parallel, and a negative displacement anti-parallel for A- and B-ion displacements.

Application of the analysis

The above analysis has identified two significant features of rhombohedral perovskite structures: (i) the inter-relationship of tilt angle $\langle \omega \rangle$ and polyhedral volume ratio V_A/V_B [(6) and Fig. 3]; (ii) the occurrence of octahedral distortions ($\Delta s \neq 0$), and their association with off-centre cationic displacements and ferroelectric properties. It is important to remark that there is virtually no correlation between the tilting and distortion of the octahedra. Any coupling between the effects would be reflected in a value of K [as defined in (3)] significantly different from one. That such a deviation from unity is not observed implies that $\langle \omega \rangle$ can be regarded as essentially independent of Δs.

The dependence of $\langle \omega \rangle$ on V_A/V_B implies that tilt angle may be chemically controlled, by varying the volumes of either the A-ion or the B-ion cation coordination polyhedra. Each of these possibilities is now considered separately, with the role of octahedral distortions discussed wherever relevant.

Control of $\langle \omega \rangle$ by the variation of V_B

An obvious system in which to study the influence of V_B on $\langle \omega \rangle$ is $PbZrO_3$–$PbTiO_3$ (PZT), for which the temperature–composition phase diagram is given in Fig. 6 (Jaffe, Cook & Jaffe, 1971). The symbols have the following meanings: P_c, cubic paraelectric phase; A_o, orthorhombic antiferroelectric phase; F_R (HT), rhombohedral high-temperature ferrolectric phase; F_R(LT), rhombohedral low-temperature ferroelectric; F_T, tetragonal ferroelectric phase. The above analysis is relevant to the F_R(LT) and F_R(HT) phases, to be found at the zirconium-rich end of the compositon range.

The F_R(HT) phase corresponds to structures in space group 160, *i.e.* PZT (0.9, ICSD Nos. 1265, 1266, 1267, 1268), PZT (0.75, ICSD No. 28927) and PZT (0.58). This space group can accommodate distorted octahedra (and, therefore, a dipole moment), but no octahedral tilting (see Table 2). Consequently the V_A/V_B ratio is fixed at 5 throughout the F_R(HT) phase field.

The F_R(LT) phase, by comparison, corresponds to structures in space group 161, *i.e.* PZT (0.9, ICSD

Nos. 1263, 1264) and PZT (0.75, ICSD Nos. 28925 and 28926). This space group can accommodate both octahedral distortions and octahedral tilting. As the titanium content increases within the F_R(LT) phase field, *i.e.* as the path from *A* to *C* in Fig. 6 is followed at room temperature, V_B falls, since Ti^{4+} is a smaller ion than Zr^{4+}. Consequently V_A/V_B increases, and the tilt angle $\langle\omega\rangle$ falls. This trend is supported by the value of $\langle\omega\rangle$ for PZT (0.75; ICSD No. 28926), 3.078°, which is smaller than the tilt angle in PZT (0.9; ICSD No. 1263) of 5.419°. Recall that the data for the PZT (0.9; ICSD No. 20625) structure are thought to be erroneous, since the calculated $\langle v_B\rangle$ valence is too high. This structure is, therefore, being disregarded in the present discussion.

A clue to the physical basis of the morphotropic phase boundary (MPB), DE in Fig. 6, is provided by a consideration of the octahedral distortions in these structures. From Table 1 it is seen that Δs increases as the titanium content increases. $\Delta s = 0.10089$ in PZT (0.9), 0.11286 in PZT (0.75) and 0.33282 in PZT (0.58), the highest of all the structures in Table 1. Thus, in PZT ($x = 0.58$), which is close to the MPB occurring at $x \simeq 0.52$, the closest O–O distances in the BO_6 octahedra are equal to $s - \Delta s = 2.536$ Å. This is close to the minimum allowed O–O separation in metal oxides, which corresponds approximately to 2.5 Å. One might suppose, therefore, that as x is increased beyond 0.58, V_B falls further, therefore, s falls. If the trend in the variation of Δs continues, Δs will increase further, so that the F_R(HT) phase will ultimately be associated with short, unfavourable O–O interactions. At a critical composition corresponding to the MPB, the tetragonal phase starts to be nucleated in preference to the rhombohedral phase, merely because it does not have the short O–O interactions which would occur in hypothetical F_R(HT) phases with $x \geq 0.52$. The observed invariance of the location of this phase boundary with temperature can also be rationalized in terms of a structural criterion involving repulsions between oxygen ions. The MPB is also further evidence for the importance of the electrostatic contribution from dipole moments in stabilizing these structures. In terms of short-range interactions alone, short O–O distances in the F_R(HT) phase could be avoided by adopting less distorted octahedra. However, this would necessarily reduce the dipole moment due to *B*-ion displacements, and the preferred option is for the system to crystallize in a different tetragonal phase, where the dipole moments are non-zero and there are no O–O interactions which would be too short. In general, therefore, the tendency for a perovskite to adopt a rhombohedral rather than a tetragonal ferroelectric phase will increase as the *B*-ion size is increased. Although $V_A/V_B = 5$ in both F_R(HT) and F_T structures, *i.e.* the polyhedral volume ratio does not discriminate between F_T and F_R(HT) phases, the F_R(HT) phase subsequently transforms to the F_R(LT) phase over the composition range $0.07 < x < 0.38$, where $V_A/V_B < 5$.

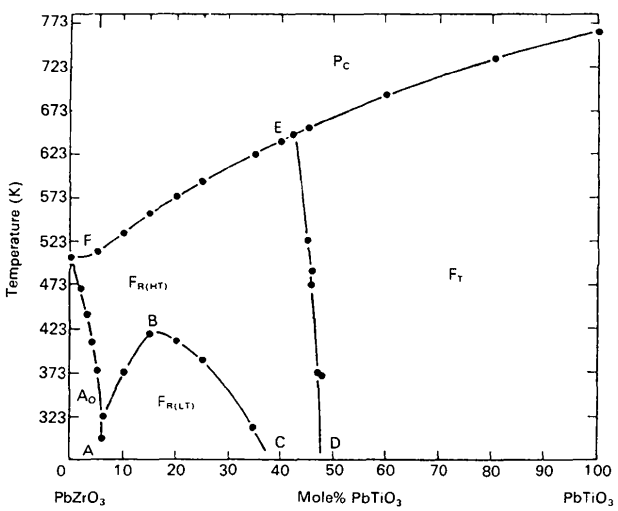

Fig. 6. The temperature–composition phase diagram of the PZT system, $Pb(Zr_xTi_{1-x})O_3$ (after Jaffe, Cook & Jaffe, 1971).

The physical basis of the phase transition from the F_R(LT)/F_R(HT) to the A_0 phase at the Zr-rich end of the composition range is less clear. Although V_A/V_B is a minimum at this side of the F_R(LT) phase field, the tilt angle of 5.419° in PZT (0.9; ICSD No. 1263) is only modest compared with some of the other rhombohedral structures in Table 1. Since the F_R(HT) phase, in which $V_A/V_B = 5$ and $\langle\omega\rangle = 0$, also transforms to the A_0 phase at low titanium content, it is unlikely that the phase transition is driven by the system acquiring a maximum allowed tilt angle for stabilization within a rhombohedral phase.

It would probably be more appropriate to analyse the A_0 phase of $PbZrO_3$, and to identify the particular features of that phase which would be destroyed either on heating or on substituting the smaller Ti^{4+} ion on the *B* sites. Such a study would provide a physical basis for understanding an A_0 to F_R(LT)/F_R(HT) phase transition, but it is outside the scope of this paper.

A detailed extension of the polyhedral volume analysis to accommodate the effects of temperature will also not be considered here. An interesting feature exists, however, in considering the F_R(LT) to F_R(HT) phase boundary, represented by *ABC* in Fig. 6. At each point on this boundary, the V_A/V_B ratio has a value exactly equal to 5, since it separates the F_R(HT) phase, where $V_A/V_B = 5$, and the F_R(LT) phase field, where $V_A/V_B < 5$. A possible way forward in modelling the F_R(LT) to F_R(HT) transition would

be to monitor the independent variation of V_A and V_B with temperature for a series of compositions within the F_R(LT) phase field. The LT to HT phase transition temperature for a given composition could then be calculated as the unique temperature at which V_A/V_B reached the value of 5.

In the absence of further experimental data, only an outline of this approach can be given at this stage. In general, it can be argued that the BO_6 octahedra are more rigid structural units than the AO_{12} polyhedra. Consequently, the coefficient of thermal expansion of the BO_6 octahedra will be less than that of the AO_{12} units. Thus, for two temperatures T_1 and T_2 within the F_R(LT) phase field, where $T_2 > T_1$, $V_{B,T2}/V_{B,T1} < V_{A,T2}/V_{A,T1}$. This trend is shown by the six structures with the $LaCoO_3$ composition in Table 1. Although they have space group 167 and not 161, which is the F_R(LT) space group, they are characterized by non-zero values of $\langle\omega\rangle$, which is the critical factor in distinguishing between the F_R(LT) and F_R(HT) phases. A consideration of the variation in V_A and V_B over the whole temperature range from 4 to 1248 K shows that V_A/V_B increases from 4.810 to 4.874, with V_B increasing by a factor of 1.072 and V_A increasing by a larger factor of 1.086. The data from PZT (0.75) also support this trend, with V_A/V_B increasing from 4.952 to 5.000 in the temperature interval between 83 and 378 K. Thus, the temperature of the F_R(LT) to F_R(HT) phase transition will be at that temperature between 293 and 378 K at which V_A/V_B first attains the value of 5. Although this argument is valid for $LaCoO_3$ and PZT (0.75), it is to be noted that the PZT (0.9) system presents a more confused picture. There is clearly a need for more experimental structural work to test the validity of this approach.

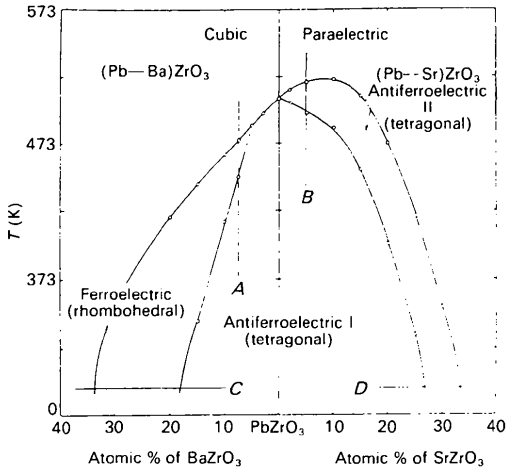

Fig. 7. The temperature–composition phase diagram of the $PbZrO_3$–$BaZrO_3$ and $PbZrO_3$–$SrZrO_3$ systems (after Shirane & Hoshino, 1954).

Control of $\langle\omega\rangle$ by the variation of V_A

Since the above analysis is based on a ratio of polyhedral volumes, V_A/V_B, it can also be applied to rhombohedral systems in which V_A is varied, instead of V_B. There is little recent work in the literature relating to A-ion substitutions in rhombohedral perovskites, but Fig. 7 (Shirane & Hoshino, 1954) serves to demonstrate the scope for such investigations. At the centre of the diagram is the composition $PbZrO_3$ in the 'antiferroelectric I' phase. Although this is described as tetragonal, subsequent investigations (Jona, Shirane, Mazzi & Pepinsky, 1957) revealed it to be orthorhombic, with the corresponding notation of A_0 in Fig. 6.

As Ba^{2+} is substituted for Pb^{2+}, V_A/V_B increases, since the ionic radius of Ba^{2+} in 12-fold coordination, $r^{XII}(Ba^{2+})$ is equal to 1.61 Å (Shannon, 1976), which is significantly larger than $r^{XII}(Pb^{2+})$, which is 1.49 Å. Conversely, the smaller radius of Sr^{2+} (1.44 Å) compared with Pb^{2+} causes V_A/V_B to decrease as Sr^{2+} is substituted for Pb^{2+} to the right-hand side of Fig. 7.

In terms of its effect on the V_A/V_B ratio, Ba^{2+} substitution for Pb^{2+} is analogous to the substitution of Ti^{4+} for Zr^{4+}: V_A/V_B in PZT (0.58) > V_A/V_B in PZT (0.75) > V_A/V_B in PZT (0.9). Thus, the polyhedral volume analysis provides a consistent description of both the $PbZrO_3$–$PbTiO_3$ and $PbZrO_3$–$BaZrO_3$ systems, in that the rhombohedral ferroelectric phase(s) are associated with a larger V_A/V_B ratio than that of unsubstituted $PbZrO_3$.

It is also consistent that Sr^{2+} substitution should not stabilize a rhombohedral ferroelectric phase, since there is an associated fall in V_A/V_B relative to the ratio in $PbZrO_3$. Although Fig. 7 implies that $SrZrO_3$ is cubic and paraelectric, as was proposed by Shirane & Hoshino (1954), subsequent work has supported the existence of $SrZrO_3$ in an orthorhombic structure (Ahtee, Ahtee, Glazer & Hewat, 1976). A calculation of V_{Sr}/V_{Zr} for this structure gives the value 4.660, as compared with a mean value for V_{Pb}/V_{Zr} of 4.962 in the $PbZrO_3$ structure (Jona *et al.*, 1957). The notion that V_A/V_B falls upon Sr^{2+} substitution is, therefore, correct.

Some recent experimental work in our laboratory has been focused on PZT (0.9), PZT (0.85) and PZT (0.8) systems with partial substitution of Ca^{2+} for Pb^{2+}. Since $r^{XII}(Ca^{2+})$, at 1.34 Å, is significantly smaller than $r^{XII}(Pb^{2+})$, the expectation was that the F_R(LT) PZT phase would be destabilized by the calcium substitution. The results of this work are to be published shortly.

Acknowledgement is made of the use of the SERC-funded Chemical Databank Service for part of the work. Acknowledgement is also due to the

Iranian Government for funding one of us (AB) for the duration of his PhD studentship.

References

AHTEE, A., AHTEE, M., GLAZER, A. M. & HEWAT, A. W. (1976). *Acta Cryst.* B32, 3243–3446.
BROWN, I. D. (1981). *Structure and Bonding in Crystals*, Vol. 2, edited by M.O'KEEFE & A. NAVROTSKY, pp. 1–30. London: Academic Press.
BROWN, I. D. & ALTERMATT, D. (1985). *Acta Cryst.* B41, 244–247.
JAFFE, B., COOK, W. R. & JAFFE, H. (1971). *Piezoelectric Ceramics*. London: Academic Press.
JONA, F., SHIRANE, G., MAZZI, F. & PEPINSKY, R. (1957). *Phys. Rev.* 105, 849–856.
MEGAW, H. D. & DARLINGTON, C. N. W. (1975). *Acta Cryst.* A31, 161–173.
MICHEL, C., MOREAU, J. M. & JAMES, W. J. (1971). *Acta Cryst.* B27, 501–503.
SHANNON, R. D. (1976). *Acta Cryst.* A32, 751–767.
SHIRANE, G. & HOSHINO, S. (1954). *Acta Cryst.* 7, 203–210.
THOMAS, N. W. (1989). *Acta Cryst.* B45, 337–345.
THOMAS, N. W. (1991*a*). *Acta Cryst.* B47, 180–191.
THOMAS, N. W. (1991*b*). *Acta Cryst.* B47, 597–608.
THOMAS, N. W. (1992). Unpublished.
THOMAS, N. W. (1993). Unpublished.
WILLIAMS, D. E. (1971). *Acta Cryst.* A27, 452–455.

Acta Cryst. (1994). B50, 560–566

Structural Relations and Tetrahedral Ordering Pattern of Synthetic Orthorhombic $Cs_2CdSi_5O_{12}$ Leucite: A Combined Synchrotron X-ray Powder Diffraction and Multinuclear MAS NMR Study

BY A. M. T. BELL

SERC Laboratory, Daresbury, Warrington WA4 4AD, England

S. A. T. REDFERN* AND C. M. B. HENDERSON

Department of Geology, The University, Manchester M13 9PL, England

AND S. C. KOHN†

Department of Physics, University of Warwick, Coventry CV4 7AL, England

(*Received* 3 *December* 1993; *accepted* 28 *March* 1994)

Abstract

A previously unknown leucite-related structure has been determined for synthetic $Cs_2CdSi_5O_{12}$. NMR spectroscopy shows that there are five distinct tetrahedral sites (T-sites) occupied by Si and one T-site occupied by Cd in the framework structure, while analysis of the synchrotron X-ray powder diffraction pattern establishes that this material is orthorhombic, *Pbca* [$R_I = 13.1\%$, $R_{wp} = 16.1\%$, $R_{exp} = 13.1\%$; eight formula units per unit cell; unit-cell parameters $a = 13.6714\,(1)$, $b = 13.8240\,(1)$, $c = 13.8939\,(1)$ Å, $V = 2625.83\,(6)$ Å^3]. Tetrahedral cation ordering rates for Si and Cd are sufficiently high for both hydrothermally and dry-synthesized samples to be fully ordered. The symmetry relations between leucites with $P2_1/c$ and *Pbca* structures are discussed and it is shown that such materials are related by a displacive phase transition, in which the number of T-sites is reduced from 12 in $P2_1/c$ to 6 in *Pbca*. The ^{29}Si MAS NMR data are, at present, less useful than the X-ray results for providing absolute T—O distances and T—O—T bond angles.

Introduction

As part of a wider attempt to understand the controls and consequences of tetrahedral cation ordering in compounds with framework structures, we are currently studying a series of synthetic leucite analogues having the general formula $X^{I}_{2}Y^{II}Si_5O_{12}$ (X = K, Rb, Cs; Y = Mg, Zn, Cd). These are related to natural leucite ($KAlSi_2O_6$) and pollucite ($CsAlSi_2O_6$) by the coupled tetrahedral framework cation substitution $2Al = Y + Si$ (Torres-Martinez & West, 1989). Such compounds are generally more amenable to tetrahedral site (T-site) analysis than Al–Si analogues and can also display significantly enhanced T-site ordering kinetics compared with the $KAlSi_2O_6$-type compound. For example, dry synthesized $K_2MgSi_5O_{12}$ leucite is cubic *Ia3d* with a dis-

* Present address: Department of Earth Sciences, University of Cambridge, Downing Street, Cambridge CB2 3EQ, England.
† Present address: Department of Geology, The University, Bristol BS8 1RJ, England.

©1994 International Union of Crystallography
Printed in Great Britain – all rights reserved